The determination of pipe contraction pressure loss coefficients for incompressible turbulent flow

P. R. Bullen*, D. J. Cheeseman*, L. A. Hussain* and A. E. Ruffell†

The accurate prediction of pipe contraction presure loss is important in the design of pipe systems, such as heat exchangers, particularly when close control of the flow distribution in a network of pipes is required. The prediction of the contraction pressure loss depends heavily on experimental data. Large discrepancies in these predictions are evident in the literature. New experimental results giving pressure loss coefficients for a range of Reynolds numbers of 4×10^4 to 2×10^5 and area ratios 0.13 to 0.7 are presented and compared with those of other workers and with predictions from a method that allows for velocity profile variation through the contraction. The results show a Reynolds number dependence. The effects of small-bore pipe inlet geometry on the loss coefficients are also examined.

Keywords: *incompressible pipe flow, pipe contractions, experimental pressure loss coefficients, analytic pressure loss coefficients*

Introduction

There is a loss of total head, due to the dissipation of energy by fluid friction, when fluids flow through a uniform pipe. Additional losses are incurred due to rapid changes in fluid velocity which occur at changes in pipe cross-section, such as a contraction.

The accurate prediction of 'minor' pressure losses in general is important when they constitute the major energy dissipation or significantly affect the fluid properties. This situation is most commonly met in heat exchangers, particularly fired heaters, boilers and cooling water condensers, where contractions exist at the entrance to the tube bundles. Contractions also occur in conjunction with enlargements, as ferrules which are often used for the close control of the flow distribution within the tube bundles. Differential ferruling is used to ensure that each tube receives a flow which is consistent with its heat input and pressure loss characteristics. Thus it is important to be able to calculate not only the absolute pressure drop through specific ferrule sizes but also the variation between closely spaced sizes. Furthermore, it is important to be able to evaluate pressure losses as a function of flow rate. Fired heaters and boilers, for example, operate between 100% and 4% MCR (Maximum Continuous Rating), which is usually equivalent to a Reynolds number range of approximately 5×10^5 to 10^4.

The use of experimentally determined dimensionless pressure loss coefficients is currently the only available approach to the prediction of contraction pressure loss. However, the paucity of contraction pressure loss coefficient data and the limited information on their experimental derivation currently make this approach unreliable.

Fig 1 shows the wide range of contraction pressure loss coefficient values predicted by previous workers. The values quoted are for a turbulent flow where the loss coefficient is supposedly independent of Reynolds number (Kays[1] does include Reynolds number effects in his prediction method). This wide variation in quoted values of loss coefficients, and the need for the accurate prediction of contraction pressure loss, have resulted in a programme of work at Kingston Polytechnic in collaboration with Babcock Power Limited to determine pipe contraction pressure loss coefficients for a range of flow and geometry conditions, to verify and extend a prediction method developed at Babcock Power Limited and presented herein.

* School of Mechanical, Aeronautical and Production Engineering, Kingston Polytechnic, Kingston upon Thames, Surrey KT2 6LA, UK
† Babcock Power Ltd, 165 Great Dover Street, London SE1 4YB, UK
Received 22 April 1986 and accepted for publication in final form on 22 December 1986

0142-727X/87/020111-08$3.00

Previous work

Introduction

The flow through the contraction is shown diagrammatically in Fig 2(a). As the fluid approaches the contraction the flow is fully developed. Disturbances are propagated upstream which cause changes in the flow from a point approximately $4d_1$ upstream of the contraction, and fully developed flow is re-established at a point approximately $14d_3$ downstream from the contraction (station 3). The stagnation head loss between stations 1 and 3 is given by

$$H_L = h_{0,1,1c} + h_{0,c} + h_{0,2c,3} \quad (1)$$

where H_L is the total stagnation head loss, $h_{0,1,1c}$ is the stagnation loss upstream of the contraction, $h_{0,c}$ is the stagnation heat loss at the contraction, and $h_{0,2c,3}$ is the stagnation head loss downstream of the contraction. The stagnation head loss can be found by extrapolating the stagnation head gradients, in the fully developed regions of the flow, to the plane of the contraction as shown in Fig 2(c). The experimental determination of the stagnation head loss for a particular contraction geometry thus requires the measurement of upstream and downstream stagnation head gradients in the fully developed regions, the stagnation head drop between stations 1 and 3, and the flow rate. The loss coefficient is a dimensionless form of this head loss.

Previous experimental work

The experimental determination of contraction pressure loss coefficients in the turbulent flow regime is reported by Benedict *et al*[2] only. However, the Reynolds number of the tests has not been specified. Some measurements in the transition region up to a Reynolds number of 7×10^3, for one area ratio of 0.28, have been reported by Kays[1]. At first sight more data appear to be available for laminar flows, but on closer examination the situation is similar. Measurements of loss coefficient are given by Astarita and Grego[3] for a range of Reynolds numbers

between 20 and 2×10^3 for one area ratio of 0.16. In all cases the contraction has been defined as sharp but has not been quantified in geometrical terms.

In all of the experimental work quoted above, the loss coefficient has been determined from measurements of static pressure and not stagnation pressure. The loss coefficient has then been defined as

$$\text{Loss coefficient } K_c = \left(\frac{\Delta P}{\rho g}\right)_{\text{loss}} \frac{\bar{V}_3^2}{2g} \tag{2}$$

where ΔP_{loss} was obtained by extrapolating to the plane of contraction the pipe wall static pressure gradients in the fully developed flow regions, then

$$\left(\frac{\Delta P}{\rho g}\right)_{\text{loss}} = h_A - h_I \tag{3}$$

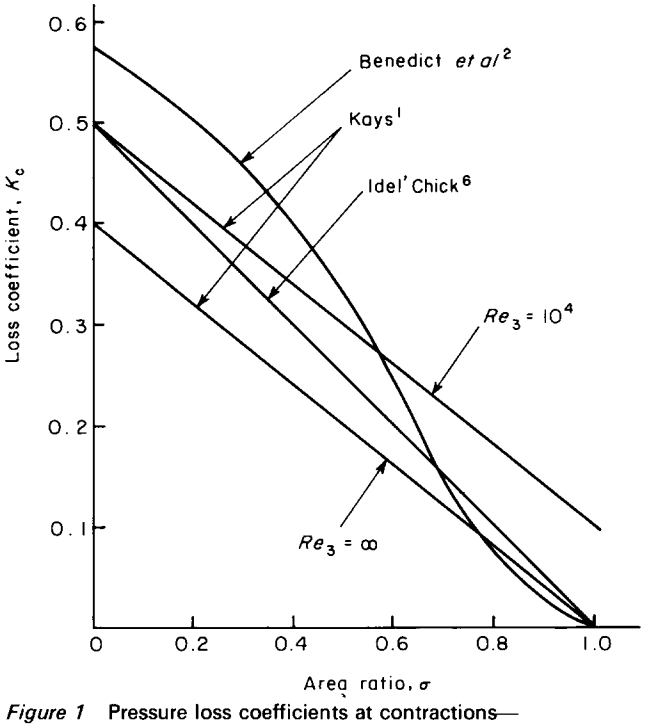

Figure 1 Pressure loss coefficients at contractions—incompressible flow

where h_I and h_A, the ideal (frictionless) and actual head drops, are defined in Figs 2(b) and 2(c), respectively. This is the definition of head loss that is generally used in current practice. However, it must be emphasized that these experimentally determined loss coefficients do not represent the loss in stagnation head as the fluid flows through the contraction, and care must be taken with their use in design procedures.

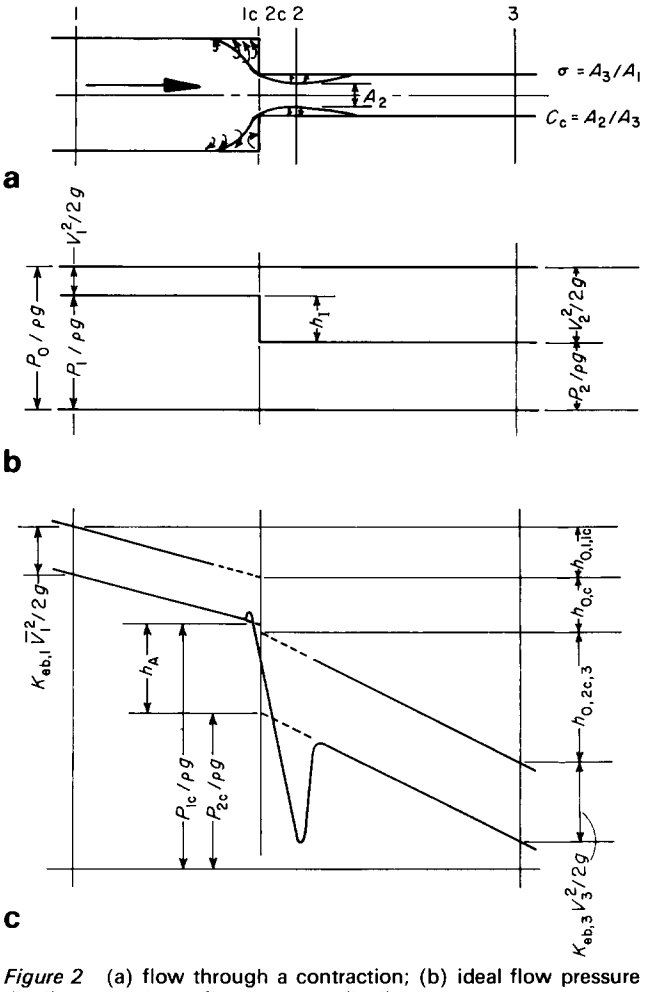

Figure 2 (a) flow through a contraction; (b) ideal flow pressure distribution; (c) real flow pressure distribution

Notation

A	Pipe cross-section area
$\bar{A}_2$	Small-bore pipe mean cross-sectional area
C_c	Coefficient of jet contraction A_2/A_3
d	Pipe diameter
F	Surface friction force
f	Friction factor
g	Gravitational acceleration
H_L	Stagnation head loss
h	Head drop
K_c	Abrupt contraction pressure loss coefficient
K_d	Momentum enhancement factor
K_{eb}	Kinetic energy enhancement factor
K'_{ti}	Total pressure loss coefficient for sharp edge contractions[5]
P	Static pressure
Q	Volumetric flow rate
R	Pipe radius
R^+	Friction Reynolds number
Re	Reynolds number
u	x-component of velocity
U^+	U/U^*
U^*	Friction velocity
V	Volumetric average velocity
v	Velocity distribution
x, y	Coordinates
y^+	Friction Reynolds number
Δ	Prefix to denote difference
λ	Edge blending factor[5]
μ	Dynamic viscosity
ρ	Density
σ	Area ratio A_3/A_1
T_0	Wall shear stress

Subscripts

0	Stagnation conditions
1	Upstream of contraction
2	Vena contracta
3	Downstream of contraction
A	Actual
c	Contraction
E	Expansion
I	Ideal
NR	Non-recoverable

Superscript

$\bar{}$	Bulk mean value

Design recommendations

The literature contains three reviews and recommendations for design methods to predict pressure losses through pipe contractions, based on experimentally determined pressure loss coefficients. These are by Miller[4], ESDU[5] and Idel'Chick[6]. There are also a number of proprietary methods which are not available in the open literature, and a number of methods which are based on the semi-theoretical derivations of loss coefficients based on the 'similar' flows.

Miller[4] defines the head loss for the flow of an incompressible fluid through a sudden contraction in line with Eq (3) above, and recommends Benedict's[2] values of loss coefficients for the turbulent flow regime.

ESDU data sheet 78007[5] deals with the pressure losses through a contraction for both compressible and incompressible fluids. ESDU quotes an expression for the static pressure drop across the contraction, due to the flow of an incompressible fluid as

$$\Delta P_{1c,2c}=\tfrac{1}{2}\rho V_3^2\left[\lambda K'_{ti}+K_{eb3}-K_{eb1}\left(\frac{A_{2c}}{A_1}\right)^2\right] \tag{4}$$

where K_{eb1} and K_{eb3} are the kinetic energy enhancement factors for circular pipes, and λ is the edge blending factor which has a value of unity for sharp edge contractions. ESDU quotes Miller's data for loss coefficients, which in fact are Benedict's original experimental data.

Idel'Chick implies that he has considered stagnation head loss in his definition of loss coefficient, but it is not clear from where his data have been obtained.

Development of an improved prediction method

Introduction

The correlations which have been presented by the various authors do not include all of the factors which should be considered to obtain an accurate value of K_c. Kays'[1] correlation appears to be the most comprehensive of the correlations put forward so far. His analysis for an abrupt contraction is incomplete in that it does not contain terms for the losses which occur at the entrance to the smaller bore and between there and the vena contracta. Furthermore, his expressions for K_d and K_{eb} are based on the 'core' flow only and are therefore limited to Reynolds numbers of the order of 10^5 and above. They are also limited by his choice of friction factor formulation.

For these reasons, it was decided to develop an improved method, the objective being to produce a procedure which was suitable for sharp-edged contractions and also capable of extension to include shaped inlets. Thus the requirements for the procedure are that it should allow for

(a) the velocity profile upstream and downstream,
(b) the area of the vena contracta, and its dependence on the geometry of the contraction,
(c) the expansion process after the vena contracta.

Analysis

The analysis considers the flow in two parts, namely the contraction from plane 1 to plane 2 and the expansion from plane 2 to plane 3 (see Fig. 2(a)).

Consider the contraction from plane 1 to plane 2, under 'ideal' flow conditions. Application of the principle of conservation of energy gives

$$\begin{aligned}\Delta P_I&=P_1-P_2\\&=\rho\frac{V_2^2}{2}-\rho\frac{V_1^2}{2}\\&=\rho\frac{V_2^2}{2}(1-\sigma^2C_c^2)\end{aligned} \tag{5}$$

which is the pressure change resulting only from the acceleration of the fluid.

Now the 'actual' static pressure is lower than in the 'ideal' case because the velocity is not constant across a diameter, more of the fluid energy being in kinetic form, and there is a loss of energy due to regions of recirculating flow between 1 and 1c, 2c and 2. Therefore

$$\Delta P_A=\rho\frac{V_2^2}{2}(K_{eb2}-K_{eb1}\sigma^2C_c^2+K_{1,2}) \tag{6}$$

where K_{eb} is defined as

$$K_{eb}=\frac{1}{A\bar{V}^3}\int_0^A v^3\,dA \tag{7}$$

and

$$K_{1,2}=\Delta P_{loss,1,2}/\rho\frac{V_2^2}{2} \tag{8}$$

The overall static pressure difference consists of a recoverable part, represented by the 'ideal' difference, and a non-recoverable part which is the remainder; this is expressed as

$$\Delta P_A=\Delta P_{NR}+\Delta P_I$$

Hence, in terms of the velocity head at the vena contracta:

$$\Delta P_{NR,c}=\rho\frac{V_2^2}{2}\{\sigma^2C_c^2(1-K_{eb1})+K_{eb2}-1+K_{1,2}\} \tag{9}$$

Now, considering the expansion from the vena contracta, plane 2, to the downstream pipe, plane 3, under 'ideal' flow conditions:

$$\Delta P_I=P_3-P_2=\rho\frac{V_2^2}{2}(1-C_c^2) \tag{10}$$

The actual pressure difference between planes 2 and 3 can be obtained from the application of the principle of conservation of momentum, assuming the pressure is constant across plane 2.

Allowance is made for the velocity profiles by defining a momentum enhancement factor:

$$K_d=\frac{1}{A\bar{V}^2}\int_0^A v^2\,dA \tag{11}$$

Applying this to the actual case:

$$P_2A_3+K_{d2}\rho V_2^2A_2=P_3A_3+K_{d3}\rho V_3^2A_3+F \tag{12}$$

where

$$F=\pi d_3\int_{L_2}^{L_3}T_0\,dL$$

which reduces to

$$\Delta P_A=P_3-P_2=\rho\frac{V_2^2}{2}(2C_cK_{d2}-2C_c^2K_{d3})-\frac{F}{A_3} \tag{13}$$

The nonrecoverable loss is defined in the same way as for the contraction; hence, in terms of the velocity head at the vena contracta:

$$\Delta P_{NRE}=\rho\frac{V_2^2}{2}\{1-2C_cK_{d2}+C_c^2(2K_{d3}-1)\}+\frac{F}{A_3} \tag{14}$$

The pressure loss at the contraction is defined by Eq (3), and explained in that subsection; hence the 'normal' pipe frictional pressure loss between planes 1 and 1c, and between 2c and 3, must be subtracted from Eqs (6) and (14), respectively. Experimental details of the flow are required to determine the positions of planes 1 and 3, and also to give information regarding the losses represented by $K_{1,2}$ and F. As a first approximation it is assumed that the pipe frictional loss is exactly balanced by the losses contained within $K_{1,2}$ and F. Possible improvements to this approximation and its justification are discussed below. The overall loss coefficient

between planes 1 and 3 therefore becomes

$$K_c=\sigma^2(1-K_{eb1})+2K_{d3}-1+\frac{1}{C_c^2}(K_{eb2}-2C_cK_{d2}) \qquad (15)$$

Evaluation of contraction coefficient C_c, momentum enhancement factor K_d, and kinetic energy enhancement factor K_{eb}

Three independent sets of measurements are available[7–9] for C_c. These are plotted in Fig 3, from which it can be seen that there are small differences between the various measurements. Unfortunately, it has not been possible to establish the flow or geometrical details of the experiments, so the differences could be real and due to variation in Reynolds number or degree of sharpness of the contraction. In the absence of this information, however, it can only be assumed that they are attributable to normal experimental scatter and, on this basis, a simple curve and expression for C_c as a function of σ are also given in Fig 3. It is known, however, that the values of C_c were obtained from measurements on freely discharging jets, but, for the present purposes, it is necessary to assume that the values are equally valid for confined jets associated with contractions in cross-section.

K_d and K_{eb} may be evaluated from the Universal Velocity Profile which is expressed in dimensionless terms as

$u^+=y^+$ for $y^+\leqslant 5$

$u^+=5.025\ln y^+-3.087$ $5<y^*\leqslant 30$

(The above coefficients are chosen to give continuity of velocity at $y^+=5$ and $y^+=30$.)

$u^+=2.5\ln y^+ +5.5$ $y^+>30$

where

$u^+=u_y/u^*$

$u^*=(T_0/\rho)^{1/2}$

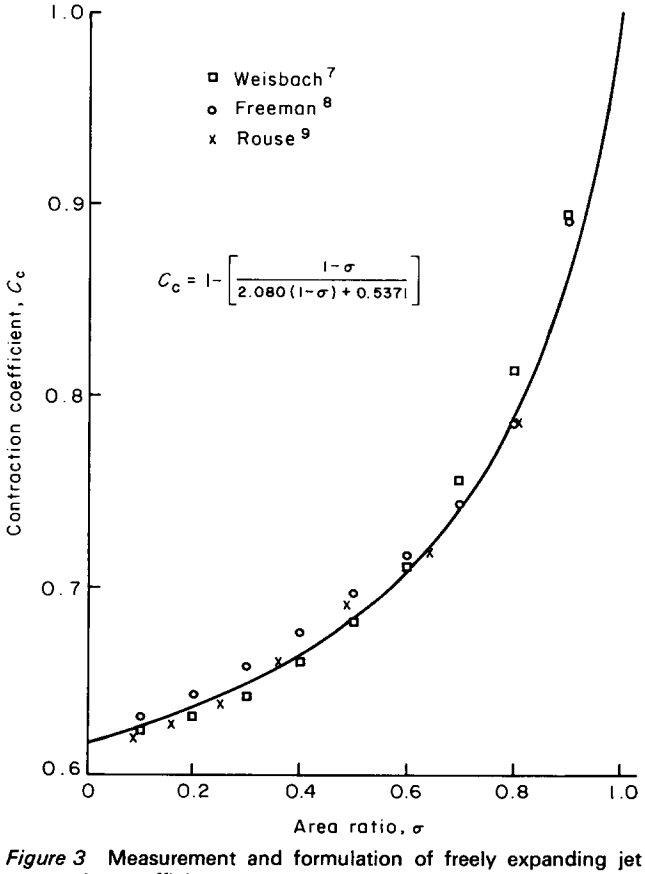

Figure 3 Measurement and formulation of freely expanding jet contraction coefficient

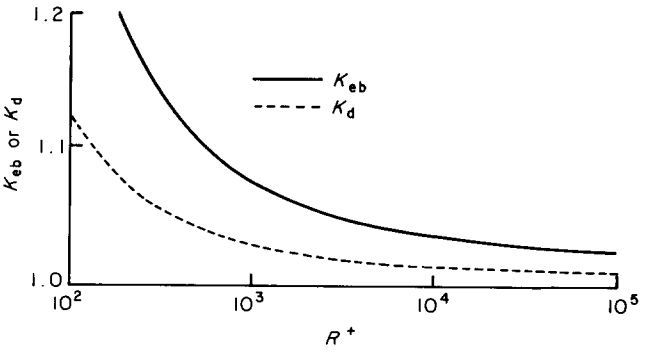

Figure 4 Variation of K_d and K_{eb} with R^+

$$y^+=\frac{y\rho u^*}{\mu};\qquad \frac{Re}{2}\left(\frac{f}{8}\right)^{1/2}=R^+$$

$$u^+=u_y/\bar{u}\left(\frac{f}{8}\right)^{1/2} \quad \text{and} \quad f=\frac{8T_0}{\rho\bar{u}^2}$$

The complete region $y^+=0$ to $y^+>30$ is considered so that Reynolds number effects are included.

From the definitions of K_d and K_{eb} (Eqs (11) and (7)) we can write integrations in dimensionless form over the radius of the tube as

$$K_d=\frac{\frac{R^{+2}}{2}\int_0^{R^+}u^{+2}(R^+-y^+)\,dy^+}{\left\{\int_0^{R^+}u^+(R^+-y^+)\,dy^+\right\}^2}$$

and

$$K_{eb}=\frac{\frac{R^{+4}}{4}\int_0^{R^+}u^{+3}(R^+-y^+)\,dy^+}{\left\{\int_0^{R^+}u^+(R^+-y^+)\,dy^+\right\}^3}$$

substituting from above

$$K_d=\frac{R^{+2}\{(Z^{+2}-7.5Z^++21.88)R^{+2}-2132R^++23272\}}{\{(Z^+-3.75)R^{+2}-126.25R^++1115.1\}^2}$$

and

$$K_{eb}=\frac{R^{+4}\{(Z^{+3}-11.25Z^{+2}+65.625Z^+-175.78)R^{+2}-30521R^++383832\}}{\{(Z^+-3.75)R^{+2}-126.25R^++1115.1\}^3}$$

where $Z^+=2.5lnR^++5.5$. Values of K_d and K_{eb} as functions of R^+ are given in Fig 4.

Note that the universal velocity profile is assumed to exist at the vena contracta as well as in the fully developed flow regions in the large- and small-bore pipes. The only alternative simple assumption is that of a uniform velocity at the vena contracta. The former was chosen as it was considered that the velocity distribution at the vena contracta would have been sufficiently influenced by the shear between the recirculating flow and the mean flow. This shear is represented by the smooth pipe friction factor. The justification of this assumption is given by the comparison of the predicted loss coefficient with experiment, in the discussion of results, below.

Improvements to the pressure loss prediction

Any improvement to the predictions given by Eq (15) will require additional information regarding the losses contained within $K_{1,2}$ and F as well as the point at which deviations from fully developed flow occur in the large-bore pipe and the point at which the flow regains its fully developed form in the small-bore pipe, in order to determine the 'normal' pipe frictional loss between planes 1 and 3.

With regard to $K_{1,2}$ one can postulate a corner loss in the form of 'eddies' located between planes 1 and 1c. No experimental data are available for pipe contractions but some are available for orifices[10,11]. The frictional loss occurring from plane 2 to the point of recovery of fully developed flow will be small in view of the expected small velocity gradients at the pipe wall due to the recirculating region. The separation and reattachment required to determine the 'normal' pipe friction loss can be estimated from our own pipe wall pressure distribution data.

Attempts to include the above data in the prediction method have failed to produce consistent results. In view of the good agreement between our experimental results and the predictions using Eq (5) (presented in Fig 9 and discussed below) the assumption that these minor losses are balanced by the 'normal' pipe friction losses, over the lengths of pipe between planes 1 and 3, appears to be justified.

Experimental work

The definition of contraction pressure loss coefficient

The discussion of previous work has demonstrated that there are ambiguities in the definition of contraction pressure loss coefficients, and that reliable experimental data are not available for use in the design procedures.

From a scientific point of view the loss in stagnation head represents the total loss in energy from the mean flow as the fluid flows through the contraction. However, as pointed out above, this stagnation head loss requires measurements of the distribution of stagnation head in the fully developed flow regions up- and downstream of the contraction.

The wall static pressure distribution along the length of the pipes forming the contraction is much easier to determine experimentally, and can be used to define a pressure loss coefficient.

Bullen and Cheeseman[12] studied the above-mentioned differences in the definition of the loss coefficient using a simple one-dimensional analysis for an incompressible flow, highlighting further difficulties with the specification of the contraction geometry and flow for both real fluids and real pipes. Their 'preferred' definition for the pressure loss coefficient was for sharp-edged contractions:

$$K_c = \frac{2g\bar{A}_2^2 h_A}{Q^2} - \left[1 - \left(\frac{A_{2c}}{A_{1c}}\right)^2\right] \tag{16}$$

Each component of the head drop, h_A and h_I, is rendered dimensionless with respect to the meaningful dynamic head $(\bar{V}_2^2/2g)$ and $(V_{2c}^2/2g)$, respectively. The ideal pressure drop at the contraction is a function of A_{2c} only, and the actual pressure drop is strongly dependent on the formation of the vena contracta, which is a function of $\bar{A}_2$ rather than just A_{2c}.

The measurements required for the experimental determination of K_c (Eq (16)) for a range of Reynolds numbers are

(i) the contraction geometry defined by A_{1c}, A_{2c} and $\bar{A}_2$,
(ii) the volumetric flow rate Q,
(iii) the static pressure drop h_A at the contraction, plane 2c (see Fig 2(a)),
(iv) fluid temperature.

The design of a test rig and the associated instrumentation must reflect these measurement requirements and provide the specified flow conditions in the test section.

The experimental rig and instrumentation

The experimental rig at Kingston was designed for a Reynolds number range of 3×10^4 to 3×10^5 (based on the large bore pipe diameter upstream of the plane of contraction) to match typical heat exchangers tube Reynolds numbers (see the Introduction).

Commissioning tests showed some fundamental problems: pressure fluctuations, flow nonuniformity, and static pressure tapping geometry. These are summarized below and are explained in detail in Refs 13 and 14.

Pressure fluctuations. Previous workers[4] have encountered difficulties in rig design to avoid these fluctuations but no details are given, only that an acceptable level of fluctuations is $\pm 0.25\%$ of the dynamic head. In attempts to improve the flow uniformity, flow straighteners were added (see Fig 5). These

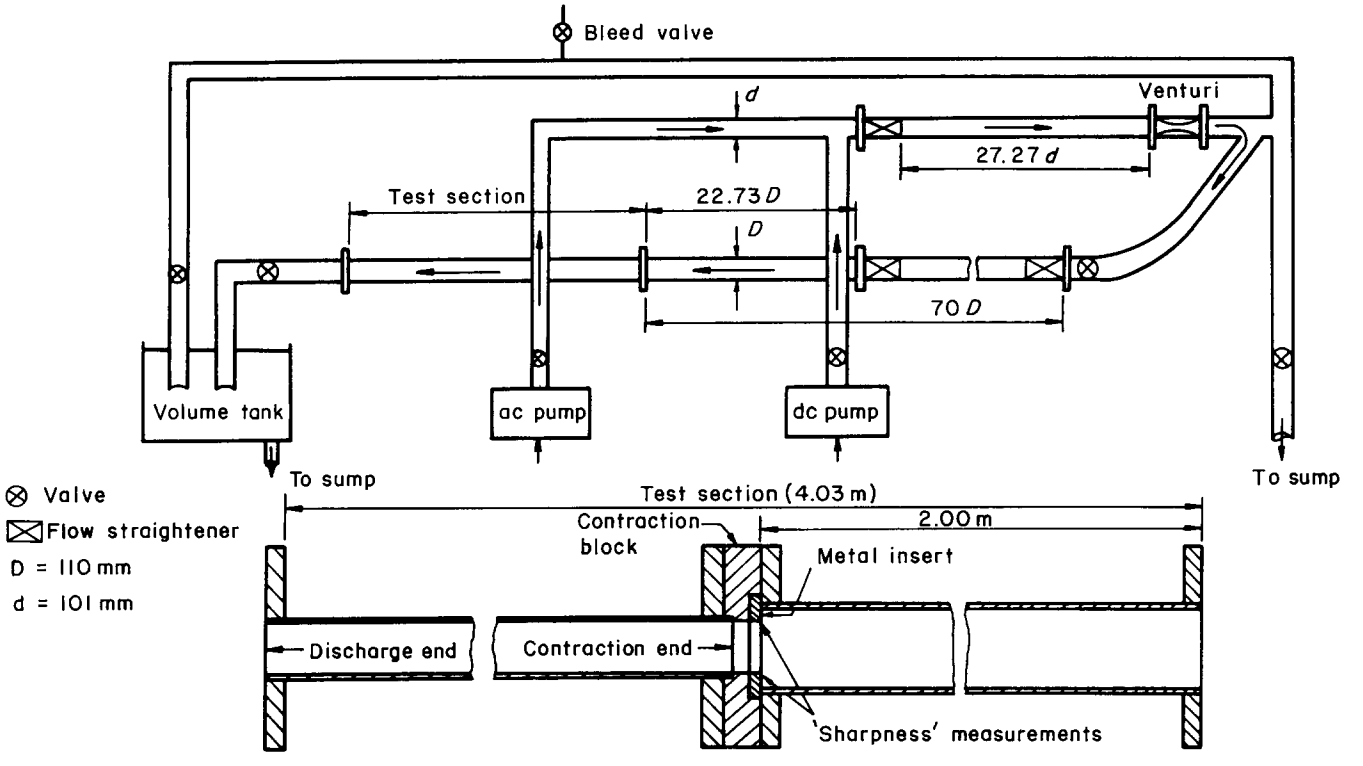

Figure 5 Schematic diagram of the test rig and test section

generated a pressure loss which provided a damping effect on the fluctuations, reducing them to $\pm 0.24\%$ of the dynamic head.

Flow uniformity. The lack of flow uniformity within the test section was originally confirmed from the differences of pressure measured around the circumference. On investigation, the lack of concentricity of the pipes forming the test section was found to be the cause. Concentricity was achieved by careful matching of the test section pipe diameters, doweling each flanged junction to ensure correct assembly, and by using a contraction block with a metal insert to form the entrance to the small-bore pipe and prevent wear during testing.

Static pressure tappings. The tappings were of 1 mm diameter with bosses glued to the pipe wall to give a ratio of length to diameter of tapping of 8. Great care was taken in drilling to ensure that it was 90° to the pipe wall, and some final finishing as suggested by Shaw[15] together with overall calibration was necessary. This calibration was achieved by replacing the upstream large-bore with a pipe of the same bore as the downstream pipe and observing any deviations from the straight line friction loss. These deviations were incorporated as calibration factors for particular tappings. At each measurement point, four circumferentially placed tappings were provided, connected in a 'Triple-T' configuration, as recommended by Blake[16].

The details of the experimental rig and test section are shown in Fig 5, with the test section geometry specified in Table 1 and Fig 6. The range of area ratios was obtained by changing the contraction block and small-bore pipe, maintaining the same large-bore pipe, hence Reynolds numbers are based on this large-bore pipe.

The instrumentation required to determine pressure loss coefficient consisted of a venturi meter calibrated against a volume tank to measure flow rate, inverted inclined manometers to measure the static pressures through the test section, and a stagnation Cr/Al thermocouple to determine water temperature.

Considering random and systematic errors, the uncertainties in measurements were typically (at high Reynolds numbers) $\pm 2.7\%$ for pressure measurement, $\pm 0.1\%$ for temperature measurement, and $\pm 1.0\%$ for the flow rate measurement. The overall uncertainty in loss coefficients based on 95% confidence limits is shown in Fig 12. This is discussed further in the following section.

Discussion of results

Pressure loss coefficients for sharp contractions

Values of pressure loss coefficient were obtained for six different area ratios and a range of Reynolds number, 4×10^4 to 2×10^5, based on the large-bore pipe diameter.

The wall static pressure profile along the test section shows the form given in Fig 7. At entry to the test section the flow is turbulent and fully developed (the velocity profile was consistent with the 1/7th power law[14]), and the pressure drop along the large-bore pipe is seen to be linear, due to friction. The friction factors obtained from these measurements were comparable with those for smooth pipes. Just upstream of the contraction a small increase in static pressure is evident. This pressure rise gives the conditions necessary to produce separation of the flow from the wall of the large-bore pipe, which will occur within the region between the contraction plane and distance d_1, approximately, upstream.

A pressure gradient across the pipe radius is required to deflect the fluid into the small-bore pipe where it accelerates as the flow area decreases. As the fluid flows into the small-bore pipe there is an almost instantaneous drop in wall static pressure, which then recovers as the flow re-attaches to the small-bore pipe. The ensuing pressure drop along the small-bore pipe is due to friction and again compares directly with the smooth-pipe friction profile.

The region of low pressure is associated with the formation of the vena contracta, although its exact position cannot be determined from the wall static pressure distribution, because of radial pressure gradients in this region. However, it is estimated

Table 1 Test section pipe diameters

Nominal pipe diameter	Mean contraction end diameter	Mean discharge end diameter	Overall mean diameter
	d_{2c}	d_d	$\bar{d}_2 = \frac{d_{2c} + d_d}{2}$
(mm)	(mm)	(mm)	(mm)
40	40.40	39.70	40.05
50	50.32	49.92	50.12
60	59.98	60.81	60.39
70	70.14	69.99	70.07
80	79.48	79.69	79.59
90	91.61	90.23	90.92
110	110.12	109.22	109.67

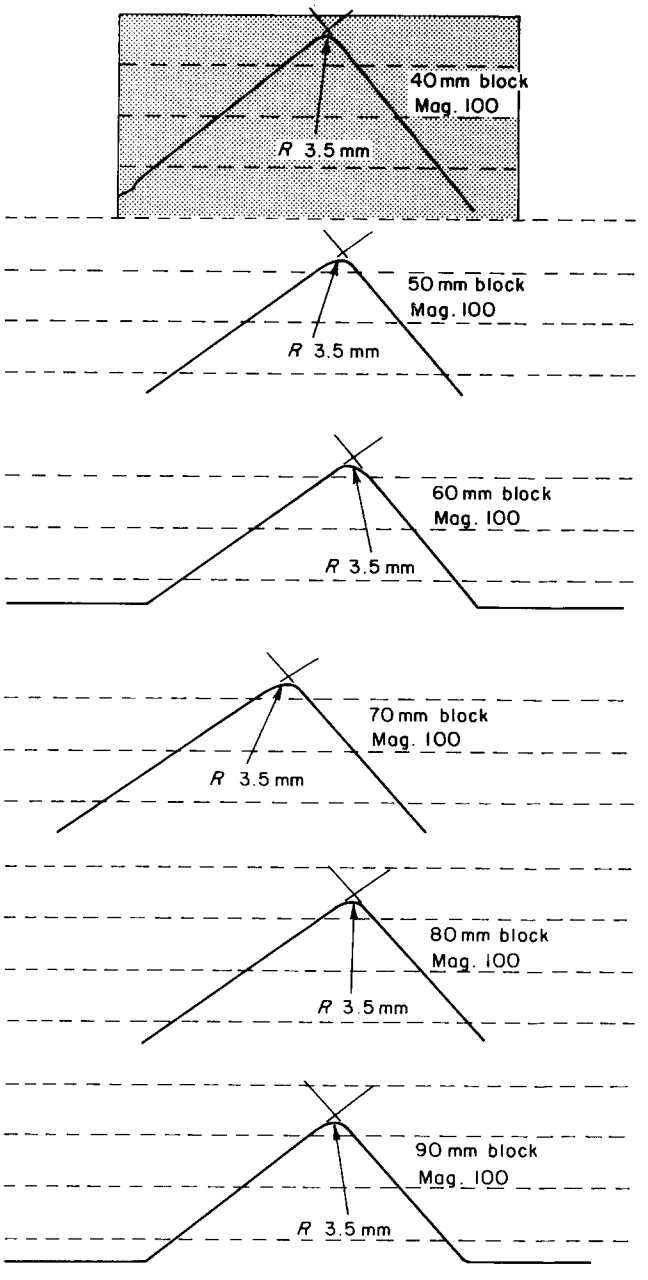

Figure 6 Metal insert edge sharpness traces

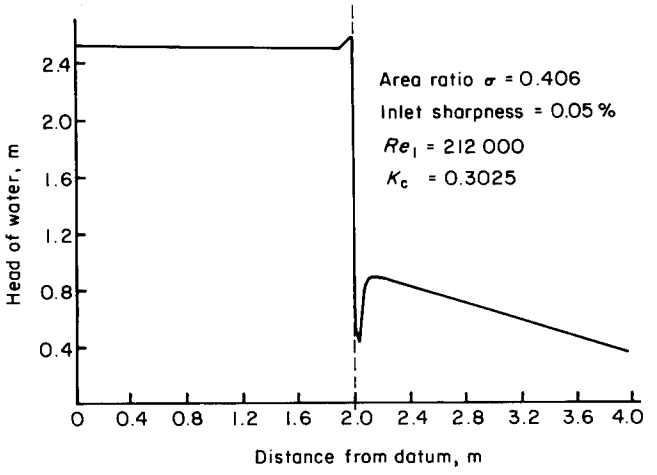

Figure 7 Typical head loss graph for the test section

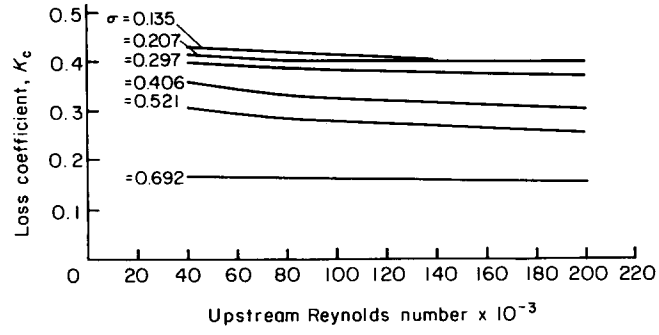

Figure 8 Variation of loss coefficient with Reynolds number—6 area ratios

that the vena contracta is in the region of 0.17 to 0.25 small bore diameters downstream from the plane of the contraction for this particular area ratio and Reynolds number. Assuming a constant static pressure across the diameter of the pipe, it can be shown, by consideration of energy conservation and mass continuity, that the ratio of vena contracta area to small-bore pipe area is of the order of 0.68, for the above conditions. This agrees closely with the values given by Benedict[2] which he adopts in a suggested calculation procedure for pressure loss coefficients.

Downstream from this minmimum pressure point, the flow expands and re-attaches to the small bore pipe wall. ESDU[5] comment that 14 small-bore pipe diameters are required before the recovery of fully developed flow is complete. The wall static pressure measured shows that the uniform head drop due to friction appears to start approximately four small-bore pipe diameters from the plane of contraction.

Values of pressure loss coefficient for six different area ratios were obtained and are shown in Fig 8. As can be seen, a small but distinct variation with Reynolds number was found over the range tested. The only other experimental work available in the open literature is that of Benedict[2] whose results for incompressible fluid flow are given as a function of pressure ratio and show no variation with this parameter. The pressure ratio is related to Reynolds number and it must therefore be inferred that no Reynolds number effects were identified.

The design recommendations by Miller[4] and ESDU[5] give constant values for the loss coefficient above a Reynolds number of 10^4. Miller's values are based on Benedict's work, and, indeed, ESDU appear to have used the same data.

The semi-theoretical approaches of Kays[1] and those presented in the section on development of an improved prediction method, attempt to include Reynolds number effects by examining changes in velocity profiles. These velocity profiles are catered for by the use of enhancement factors. The experimentally determined values are compared with the predictions made above and are shown in Fig 9. The form of variation shown by the theoretical method is found to be similar to that found experimentally, although the details differ as can be seen in Fig 9. It must be emphasized that even though the predicted values are not in total agreement with the experimentally determined values they still do fall within the calculated experimental uncertainty band which is shown in Fig 12 and discussed below.

These differences probably result from the assumptions of the size of the vena contracta and the velocity profile, which are a necessary input to the prediction analysis. The analysis has used 'similar' flows such as free jet and orifice data in an attempt to define the vena contracta. At lower area ratios the confining effect of the small-bore pipe is more dominant than for higher area ratios, and hence the detailed flow structure in the region of the vena contracta cannot be predicted exactly from these 'similar' flow conditions.

There is more favourable agreement between the experimentally determined values of loss coefficient and the semi-theoretical method presented herein than with previous workers' experimentally determined curves. As can be seen in Fig 10, the differences can be as high as 25% at an area ratio of 0.135. The difference in experimental values could be due to the flow conditions in the test section, the test section geometry, or the neglect of Reynolds number effects over the range tested; however, as the specific details have not been given, the exact reasons cannot be ascertained.

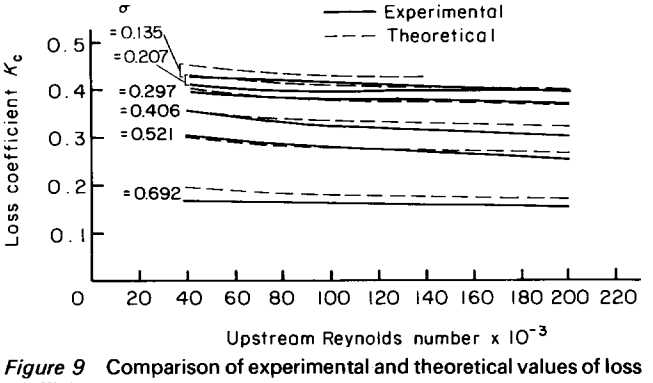

Figure 9 Comparison of experimental and theoretical values of loss coefficients

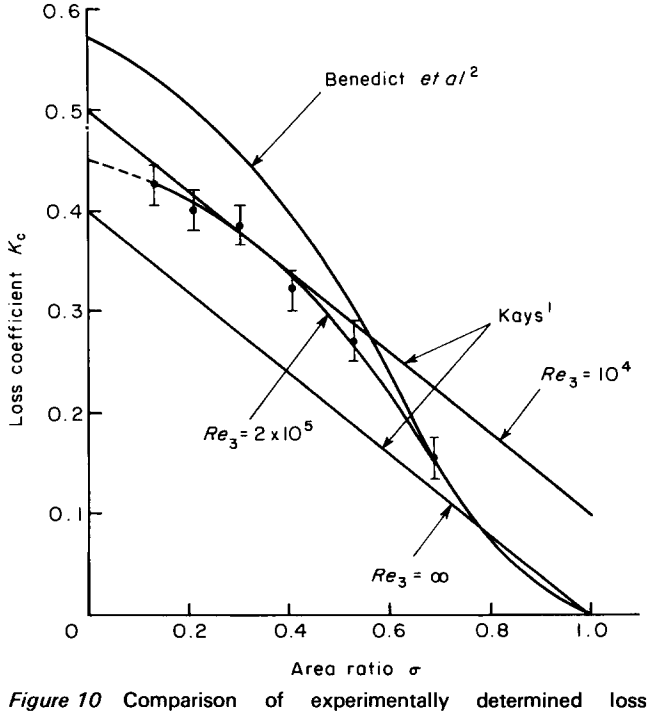

Figure 10 Comparison of experimentally determined loss coefficients

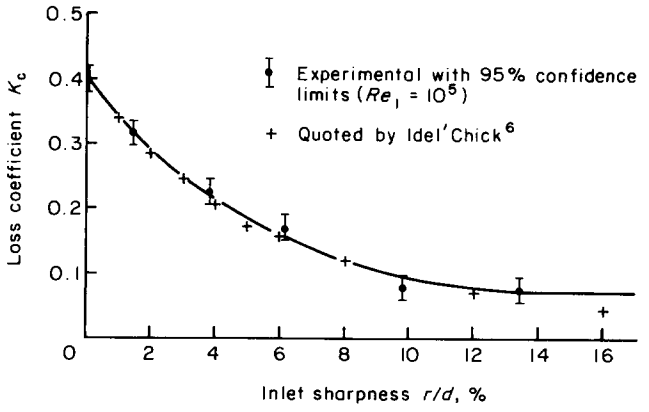

Figure 11 Variation of loss coefficient with inlet sharpness

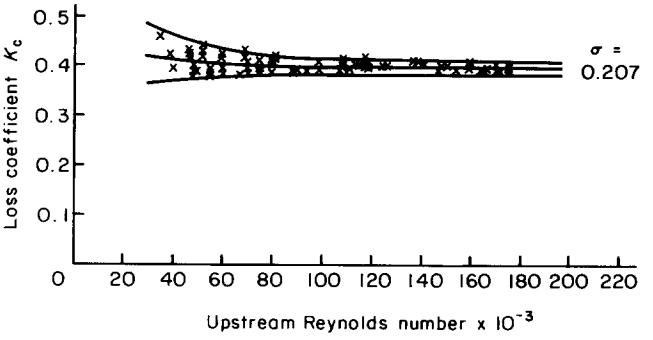

Figure 12 Uncertainty in experimental results

Effects of small-bore pipe inlet geometry

The sharpness of the contraction defined as the percentage rounding of the inlet to the small bore compared with the pipe diameter is of great importance, since any deviation from an absolutely sharp inlet results in a lower loss coefficient value. Previous workers omit to mention its effects or define their contraction geometry exactly, yet design procedures do refer to it. The only information available is that provided by Idel'Chick[6], but he does not refer to the original data from which this has been taken and it is therefore not clear whether his values are experimental or theoretical.

The effects of the inlet sharpness have been investigated at Kingston on an area ratio of 0.207. It was found that the loss coefficient is heavily dependent on the inlet sharpness. The results are shown in Fig 11 for one particular Reynolds number, where they are also compared with values given by Idel'Chick[6]. Close agreement is evident. The Reynolds number effect increased with the increasing r/d ratio. This was to be expected since a sharp inlet acts as a turbulence generator.

Error analysis

The values of pressure loss coefficient shown in Fig 8 are those obtained experimentally for small-bore inlet geometries (sharpness) of 0.035 mm (equivalent to 0.038% and 0.087% for the largest and smallest small-bore pipes, respectively). An experimental result is only useful if a statement of uncertainty or confidence is placed on the results. The uncertainty analysis[14] was applied to the experimental measurements of the pressure loss coefficient as discussed earlier and the test section geometry. The results of this analysis are shown in Fig 12 (just one case for clarity) as an error band with 95% confidence limits. It should be noted that the uncertainty in the loss coefficient increases rapidly at small Reynolds numbers for the larger area ratios, mainly on account of the increase in uncertainty of the pressure measurements. This could be overcome by increasing the test section length but, at present, lack of space prevents this.

Conclusions

(i) The values of pressure loss coefficient obtained from wall static pressure distribution show a Reynolds number dependence over the range tested (4×10^4 to 2×10^5), this dependence increasing with decreasing Reynolds number.

(ii) There is good agreement between the experimental values of pressure loss coefficients and the predictions based on the analysis herein. The small differences could be due to the confining effect of the small-bore pipe on flow development downstream of the contraction, invalidating the use of 'similar' flow data, and to the velocity profile assumption at the vena contracta. This is now being investigated by LDA velocity profile measurements and will be reported in the future. The part of the calculation procedure dealing with the expansion process from the vena contracta is also valid for the general case of flow through expansions in cross-section.

(iii) The values obtained show differences from previous workers' experimental results, the variation being as high as 25% for an area of 0.135.

(iv) The contraction sharpness has a significant effect on pressure loss coefficient.

(v) The results for pressure loss coefficient presented are accurate to $\pm 5\%$ to $\pm 10\%$ at high Reynolds number for the smallest and largest area ratios, respectively. The results at lower Reynolds number should be used with caution.

Acknowledgements

The overall project is supported by SERC and Babcock Power Limited, and this is gratefully acknowledged.

References

1 Kays, W. M. Loss coefficients for abrupt changes in flow cross-section with low Reynolds number flow in single and multiple tube systems. *Trans. ASME*, 1950, **72**, 1067–1074

2 Benedict, R. P., Carlucci, N. A. and Swetz, S. D. Flow losses in abrupt enlargements and contractions. *Trans. ASME, J. Eng. for Power*, 1966, **88**, 73–81

3 Astarita, G. and Grego, G. Excess pressure drop in laminar flow through sudden contractions. *Int. Eng. Chm. Fundam.*, 1968, **7**(1), 27–31,

4 Miller, D. S. Internal flow—a guide to losses in pipe and duct systems, BHRA, 1971

5 ESDU Pressure losses in flow through a sudden contraction of duct area, Data Sheet 78007, 1977

6 Idel'Chick, I. E. Handbook of hydraulic resistance, US Atomic Energy Comm., AEC-tr-6636, 1966

7 Weisbach, J. *Mechanics of engineering*, translated by Coxe, E. B., Von Nostrand Book Co., New York, 1872, 821

8 Freeman, J. R. The discharge of water through fire hoses and nozzles. *Trans. ASCE*, 1888, **21**, 303–482

9 Rouse, H. *Elementary fluid mechanics*, John Wiley & Son, New York, 1946, 265

10 Tuve, G. L. and Sprenkle, R. E. *Instruments*, Nov. 1933, **6**, 201–206

11 BS 1042. Methods of measurement of fluid flow in closed conduits, Part 1: pressure differential devices, 1981

12 Bullen, P. R. and Cheeseman, D. J. The definition of pipe contraction pressure loss coefficient for incompressible flow. Kingston Polytechnic, Internal Paper, 1983

13 Bullen, P. R., Cheeseman, D. J. and Gerami-Tajabadi, H. An investigation of the flow through pipe contractions. Polytechnic Symposium Leicester, Nov. 1982

14 Gerami-Tajabadi, H. The determination of pressure loss coefficients for an incompressible flow through pipe contractions. MPhil Thesis, Kingston Polytechnic, 1985

15 Shaw, R. The influence of hole dimensions on static pressure measurements. *J. Fluid Mech.*, 1960, **7**, 550–564

16 Blake, K. A. The design of piezometer rings. *J. Fluid Mech.*, 1976, **78**, 415–428